



Adhesion of thermal oxide scale formed on silicon-containing hot-rolled steel oxidised in oxygen

Wannapha ISSAARD¹, and Thanasak NILSONTHI^{1,*}

¹ High Temperature Corrosion Research Centre and Department of Materials and Production Technology Engineering, Faculty of Engineering, King Mongkut's University of Technology North Bangkok, 1518, Pracharat 1 Road, Wongsawang, Bangsue, Bangkok, 10800, Thailand

*Corresponding author e-mail: thanasak.n@eng.kmutnb.ac.th

Received date:

29 December 2022

Revised date

5 March 2023

Accepted date:

2 April 2023

Keywords:

Adhesion;
Oxide scale;
Hot-rolled steel;
Silicon

Abstract

Defects can be caused by the thermal oxide scale that forms on the surface of steel during the hot rolling process. The oxidation and adhesion of scale on silicon-containing hot-rolled steel were investigated in a flowing 20% O₂-N₂ gas mixture at 900°C. Scale spallation was observed using a tensile testing machine equipped with a CCD camera. The thickness of the scale was 3.45 μm for the higher silicon steel and 4.86 μm for the lower silicon steel. The oxide scale consists of hematite, magnetite, wustite, and iron. The strain that caused the first spallation was used to calculate the mechanical adhesion energy, which indicated the behaviour of the scale adhesion on a steel substrate. The strain initiation of the first spallation of scale on higher silicon steel was 5.57% which was higher than 4.57% for lower silicon hot-rolled steel. The calculated adhesion energy on the studied steel was shown to be in the range of 281 J.m⁻² to 334 J.m⁻². It can be noted that the higher amounts of silicon content in hot-rolled steel increased steel-scale interface adherence. This was due to the precipitated silicon oxide near steel-scale interface might be exhibited as a reinforcing phase.

1. Introduction

The hot-rolled steel has been widely applied to industries, such as structural parts, agricultural instruments, metal structures, stampings, and automobile frames. The hot rolling operation comprises heating the furnace, descaling on a primary scale, roughing the mill with reversal, descaling on a secondary scale, finishing the mill, and cooling on the run-out table. The hot rolling process is operated at high temperature with ambient temperature. The temperature of steel passing through the reheating furnace is in the range of 1200°C to 1300°C before the reversing at the roughing mill. The steel is passed through a hydraulic descaler to remove the primary scale after the reheating furnace. The steel is subjected to a roughing mill to reduce its thickness from 160 mm to 250 mm to 26 mm to 40 mm. During the roughing mill, a secondary scale is formed, which is muted to remove before the finishing mill. The seven finishing mills are used to reduce the steel thickness by product specification. The steel is cooled down to approximately 650°C by a cooling bed in the air [1-5] and then coiled in a down-coiler process. A ternary scale is always formed till room temperature. The surface quality of hot-rolled steel is ultimately determined by the tertiary scale formed at the finishing mill. However, during the hot rolling line, the steel certainly becomes oxidized because of the air conditioning and high temperature. An oxide scale is formed on the steel surface by high-temperature oxidation exposed to an oxygen atmosphere [6-14]. The oxide characteristic varies depending on the chemical composition, atmosphere, and hot rolling parameters. An alloying element is added to the steel to improve its mechanical properties. The steel is mainly iron with some alloying elements

such as carbon, silicon, phosphorus, sulfur, etc. These alloying elements impact the formation and adhesion of scale on hot-rolled steel. Generally, the oxide layer is mainly composed of three iron oxides, which are hematite (Fe₂O₃), magnetite (Fe₃O₄), and wustite (FeO) [5-9,15-22]. In the case of silicon-containing steel, silicon exists on the oxide scale in the form of fayalite (Fe₂SiO₄) at a temperature above 750°C at the scale-steel interface and appears in the wustite matrix [8,11,12,15,21-26]. The silicon-containing steel has a strong adhesion between fayalite and the steel substrate, making it difficult to descale as required. The oxide scale morphology influences the final steel surface quality and also the scale-removing process. Currently, the hydraulic descaling process is used to descale during the hot rolling line and hydrochloric acid is used after the hot rolling line to remove the oxide scale. The various techniques have been used to measure the adhesion of the scale on steel substrates, such as the indentation test [27-29], the inverted-blister test [26,30-32], and the tensile test [33-38]. In the case of the tensile test, the scale spallation is always identified as scale adhesion, which can be followed to calculate the mechanical adhesion energy. The tensile test has been developed in our group. During tensile loading, a strain at the first spallation of scale has been critically linked to scale adhesion [37-40]. However, a few studies have been focused on the scale of silicon-containing hot-rolled steel. A better understanding of scale adhesion on silicon-containing hot-rolled steel is important to the steel industry. The purpose of this research is to investigate the adhesion of thermal oxide scale formed on silicon-containing hot-rolled steel oxidised in an oxygen atmosphere. The adhesion behaviour of oxide scale on silicon-containing hot-rolled steel is assessed by a tensile testing machine

with a CCD camera to monitor scale failure during the tensile loading. The result is always valuable to the hot-rolled steel industry.

2. Experimental

The material used in this study is hot-rolled low-carbon steel strips with a thickness of 3.2 mm, which is manufactured on a hot-rolling line at 860°C and 610°C for finishing and coiling temperatures respectively. The silicon-containing hot-rolled steel is 0.026 wt% Si (lower silicon steel) and 0.193 wt% Si (higher silicon steel), with chemical compositions as shown in Table 1. The dimension of the specimen for the oxidation test is shown in Figure 1, as accorded to the ASTM E8M standard. The specimen is continuously polished from 120 grit to 1200 grit SiC grinding papers, placed in an acetone solution with an ultrasonic cleaner, dried in the air, and rapidly placed in the horizontal furnace. The specimen is exposed to oxidation at 900°C for 2 min in a 20% O₂-N₂ mixer atmosphere with a flow rate of 6 l/min. The oxide scale morphology and elemental analysis are used by a scanning electron microscope (SEM) and an energy dispersive spectrometer (EDS). The oxide phase is defined using X-ray diffraction (XRD) on the Cu K α radiation ($\lambda = 0.15406$ nm) with 0.02 degree/step and 0.5 s/step. The adhesion test is performed using a tensile testing machine with a load of 10 kN. The test is performed at room temperature. The tensile specimen is strained at a strain rate of 0.04 s⁻¹. Scale failure during straining is monitored using a high-magnification lens equipped with a CCD camera. A video processing is carried out at a resolution of 640 pixels \times 480 pixels. The image framework program is used to control image acquisition with a frame rate of 7.5 frames/s. The tensile testing machine setup is shown in Figure 2.

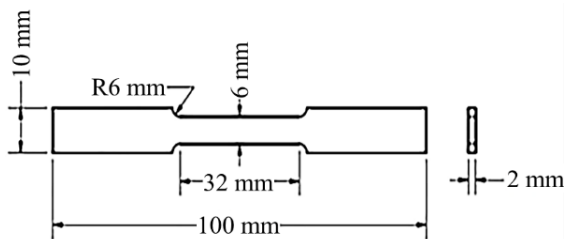


Figure 1. Dimension of specimen for the oxidation test.

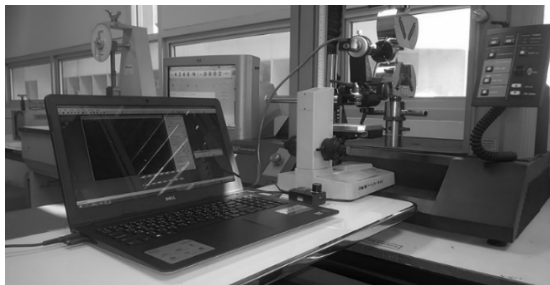


Figure 2. Tensile testing machine with observation set.

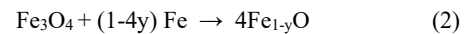
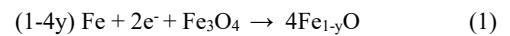
Table 1. Chemical compositions of the hot-rolled steel (wt%).

Hot-rolled steel	Composition (wt%)							
	C	Si	Cu	Mn	Al	P	S	Fe
0.026 wt% Si	0.159	0.026	0.040	0.521	0.039	0.008	0.008	Bal.
0.193 wt% Si	0.165	0.193	0.047	0.542	0.036	0.011	0.007	Bal.

3. Results and discussion

3.1 Oxide scale formation

The oxidation was performed in a horizontal furnace at 900°C for 2 min in a 20% O₂-N₂ mixer atmosphere. Figure 3 shows a SEM micrograph of the hot-rolled low-carbon steel cross-section. The thicknesses were determined at five different points along the oxide layer. Lower silicon steel has an average scale thickness of 4.86 μ m with a standard deviation of 0.29 μ m, while higher silicon steel has a thinner scale of 3.45 μ m with a standard deviation of 0.12 μ m. The formation of an oxide layer on a steel substrate in 20% O₂-N₂ atmosphere requires iron ion outward diffusion and oxygen ion inward diffusion. The oxide phases in the studied samples were identified using X-ray diffraction (XRD) as shown in Figure 4. The oxide phases were found to be hematite (Fe₂O₃), magnetite (Fe₃O₄), wustite (FeO), and iron (Fe). According to the Fe-O phase diagram given in Figure 5, wustite was unstable at temperatures below 570°C causing it to transfer into two layers of magnetite and iron. The wustite was thermodynamically stable at temperatures above 570°C and increased as the reaction progressed, in which the Fe²⁺ species diffuses rapidly at high temperatures. The eutectoid reaction of the wustite transformation was presented in Equations (1) and (2).

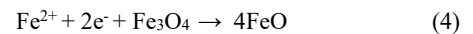


The iron ions diffuse outward during oxidation to form FeO, Fe₃O₄, and Fe₂O₃ as shown in Figure 6. The interface reaction of their iron oxide as followed,

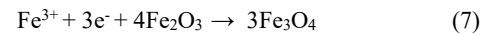
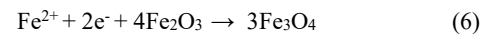
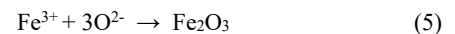
At Fe-FeO



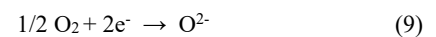
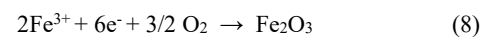
At FeO-Fe₃O₄



At Fe₃O₄-Fe₂O₃



At Fe₃O₂-O₂



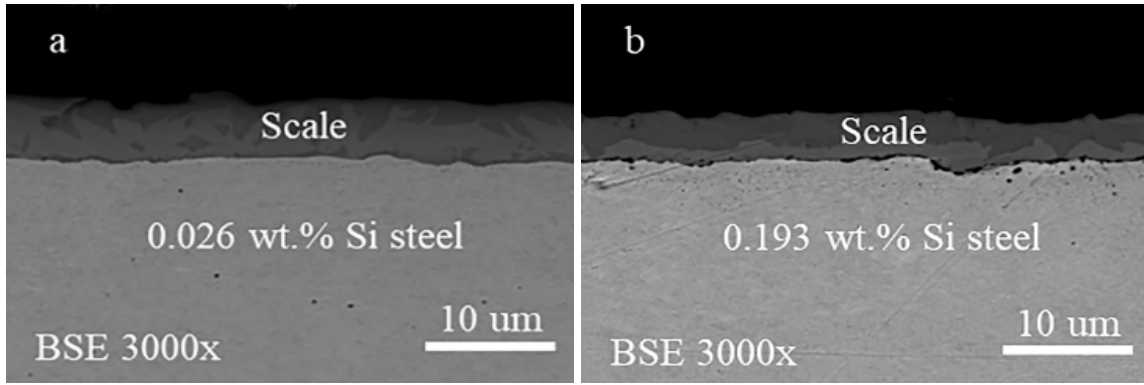


Figure 3. SEM micrographs of the lower silicon steel (a) and higher silicon steel (b) oxidised in 20% O₂-N₂ at 900°C.

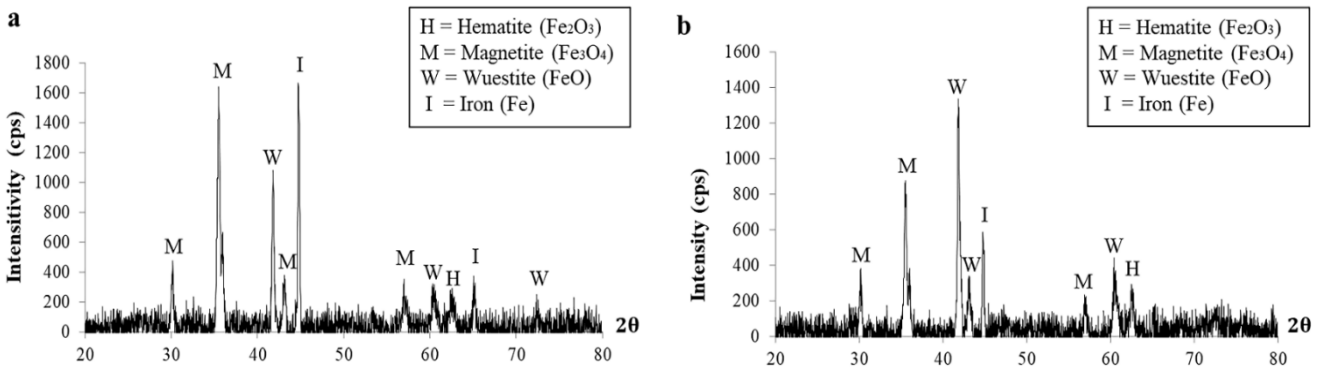


Figure 4. XRD patterns of the lower silicon steel (a) and higher silicon steel (b) oxidised in 20% O₂-N₂ at 900°C.

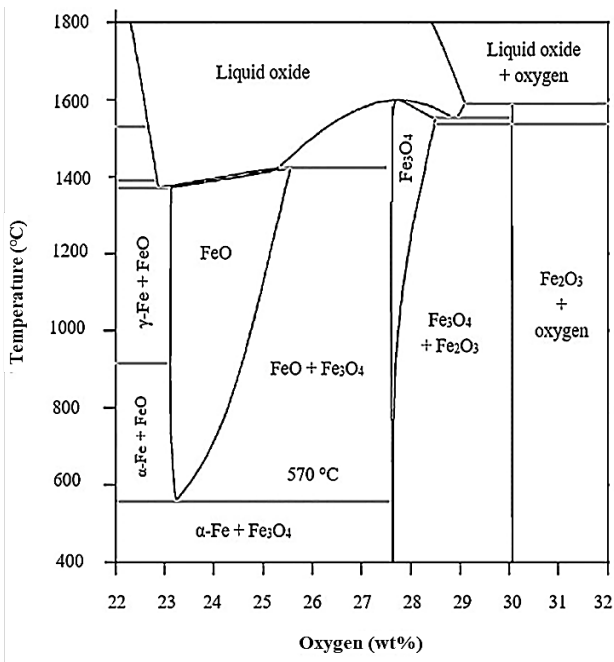


Figure 5. Fe-O phase diagram [42].

The formation of wustite and magnetite was controlled by the transport of metal cations outward, while that of hematite was controlled by the inward transport of oxygen anions [2]. Figure 7 shows a cross-sectional diagram of a growing oxide layer. The oxidation process consists of oxygen transfer to the scale-oxygen interface and metal transfer from steel to the steel-scale interface. The oxide scale was continuously grown by metal and/or oxygen transfer via the scale [41].

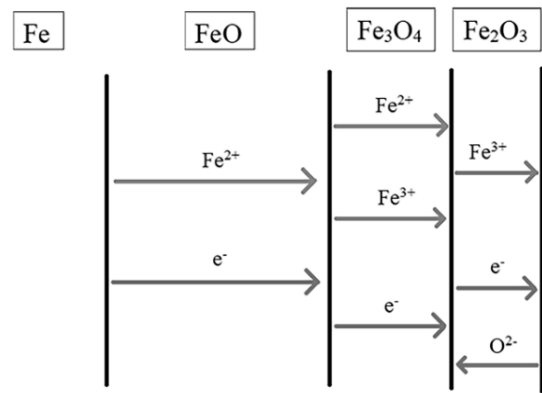


Figure 6. The diffusion of iron ions occurs during oxidation above 570°C [43].

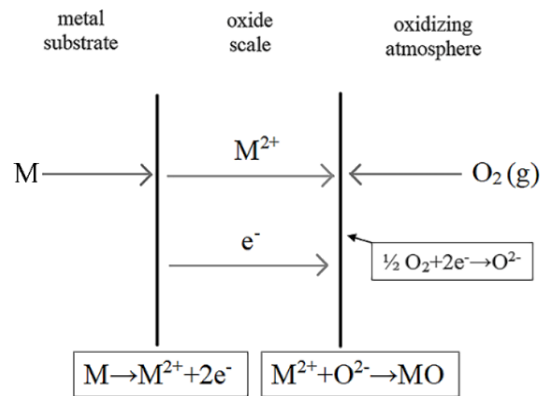


Figure 7. Reaction and transport processes involve the growth of oxide [43].

3.2 Oxide scale adhesion

Figure 8 shows the progression of scale failure on the hot-rolled steel during the tensile test. The high-magnification lens equipment and a CCD camera were used to monitor the scale spallation during straining. The dark area in Figure 8 indicated that the area of oxide scale spalled out, while the bright area indicated the area of oxide scale. The spallation of oxide scale increased as the tensile strain increased. Figure 9 shows the spallation ratio of scale on silicon-containing hot-rolled steel as the imposed strain. The spallation ratio was calculated by dividing the area of oxide scale spalled out by the total area of the image. The result shows that the spallation ratio of the 0.026 wt% Si steel was higher than that of the 0.193 wt% Si steel. The strain at the first spallation was commonly used to calculate the mechanical adhesion energy. The strain at the first spallation of lower silicon steel was 4.57%. This value was less than the higher silicon steel as shown at 5.57%. It was found that the spallation ratio and strain at the first spallation of high-silicon steel were significantly indicated. It can be noted that the Si alloying element added to hot-rolled steel was clearly causing enhanced scale adhesion.

The scanning electron microscope (SEM) with energy dispersive spectroscopy (EDS) was used for microscopic analysis of silicon-containing hot-rolled steel as shown in Figure 10 and Figure 11. Elemental analysis of the surface in SEM was conducted using EDS, which measures the energy and intensity at the steel-scale interface of the specimen after a tensile test. Elemental analysis information was presented in Table 2. It was observed that the peaks of C, O, Si, and Fe at the steel-scale interface. However, it can be noted that a higher elemental intensity of oxygen and silicon in the 0.193 wt% Si steel was clearly observed. This indicates silicon oxide existed at the steel-scale interface of the higher-Si hot-rolled steel. At high temperatures, silicon has a significant impact on scale formation and adhesion. It can be found in a wustite-fayalite mixture, which acts as a barrier at the steel-scale interface and can reduce the oxidation rate. Wustite with a fayalite layer close to the steel surface was making descaling difficult [8,11,12,15,21-26].

As explained by Gibbs free energy, the silicon element in hot-rolled steel can control fayalite formation by first reacting with oxygen during initiating oxidation to form silicon oxide. Then, silicon oxide becomes porous, allowing iron to diffuse and form fayalite. However, the amounts of silicon oxide increased as the silicon content in steel increased. It can be pointed out that the silicon oxide that precipitates within scale and sometimes precipitates as internal oxidation in steel substrates can approach the highest adhesion of scale. The presence of silicon can form silicon oxide, which was precipitated within iron oxide and its steel substrate and thus does not need to be added to steel for easy de-scaling. However, this might perhaps even be exploited to produce high-scale adhesion on hot-rolled steel as requested for products such as structural steel, pipes, tanks, etc. The precipitated silicon oxide along the steel-scale interface might be exhibited as a reinforcing phase if smooth and strong precipitated silicon oxide can be produced. However, scale adhesion may depend on abundant elements such as carbon, iron, and oxygen. For this reason, it was a matter of discussion as to how oxide scale increases adhesion to steel substrates.

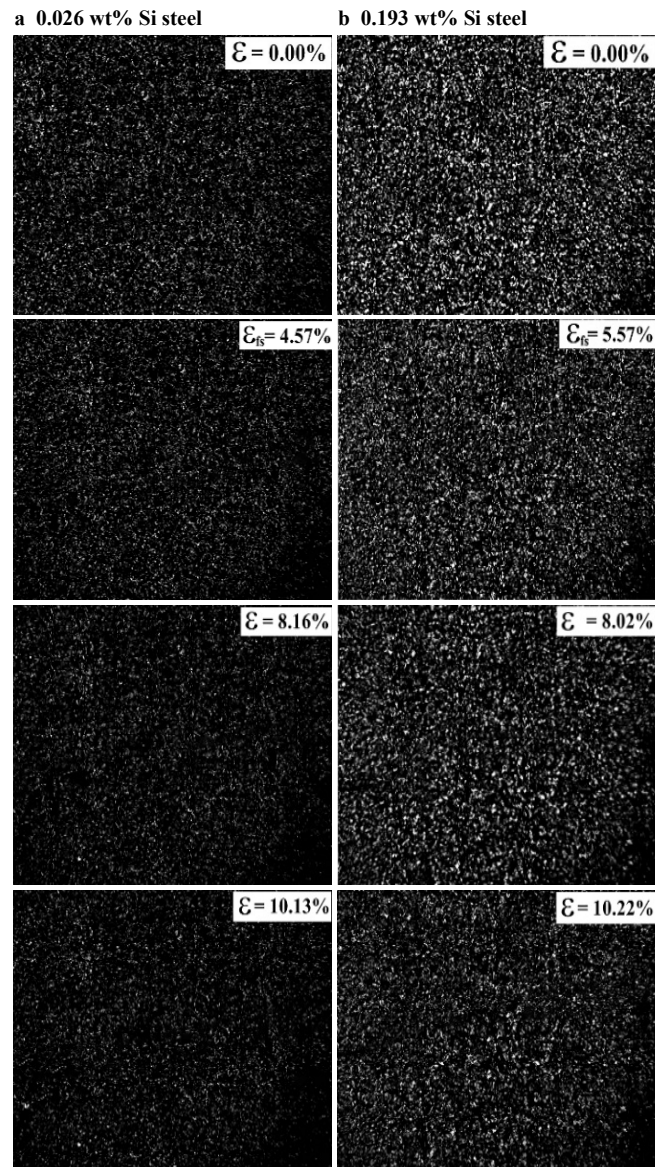


Figure 8. Evolution of the scale failure on the lower silicon steel (a) and higher silicon steel, and (b) as the imposed strain.

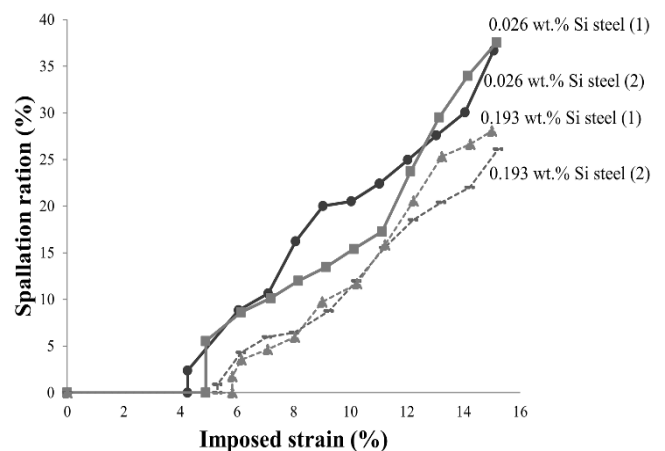


Figure 9. Spallation ratio of scale on silicon-containing hot-rolled steel as the imposed strain.

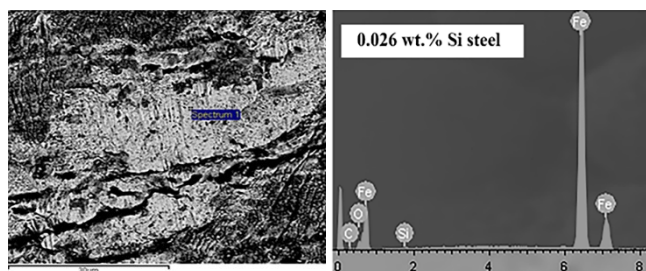


Figure 10. Oxide scale (dark area) and steel substrate (bright area) of lower silicon steel (left) with EDS pattern (right) investigated at steel-scale interface after tensile test.

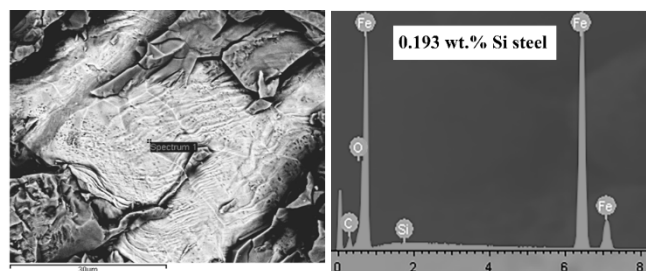


Figure 11. Oxide scale (dark area) and steel substrate (bright area) of higher silicon steel (left) with EDS pattern (right) investigated at steel-scale interface after tensile test.

Table 2. Relative concentration of the elements at the steel-scale interface.

Hot-rolled steel	Element (wt%)			
	C	O	Si	Fe
0.026 wt.% Si	7.28	0.27	0.03	92.42
0.193 wt.% Si	6.50	0.8	0.28	92.42

Table 3. Oxide formed and Gibbs free energy calculated at 900°C.

Oxide formed	Reactions	Gibbs free energy (kJ.mol ⁻¹)
FeO	2Fe + O ₂ → FeO	-381.74
SiO ₂	Si + O ₂ → SiO ₂	-718.58

Table 4. Scale thickness, strain initiating the first spallation, and mechanical adhesion energy of silicon-containing hot-rolled steel.

Hot-rolled steel	Scale thickness (μm)	Strain initiating the first spallation (%)	Mechanical adhesion energy (J.m ⁻²)
0.026 wt.% Si	4.86	4.57	281
0.193 wt.% Si	3.45	5.57	334

4. Conclusions

This research investigated the adhesion of the oxide scale to 0.026 wt% and 0.193 wt% Si hot-rolled steels oxidised in a 20% O₂-N₂ atmosphere. The oxide scale formed on silicon-containing hot-rolled steel consists of hematite, magnetite, and wustite with iron. The oxide containing silicon was formed near the steel-scale interface of 0.193 wt% Si steel. Scale thicknesses formed on 0.193 wt% Si steel were thinner than those formed on 0.026 wt% Si steel. The higher silicon content of 0.193 wt% Si hot-rolled steel can form silicon oxide precipitate along the steel-scale interface. This increased steel-scale adhesion of a high-silicon hot-rolled steel. Silicon oxide behaves as a reinforcing phase that resists external stresses. As a result, the adhesion of the scale was increased. This information was particularly

The Gibbs free energy can be calculated by the Equation (10), and the information was shown in Table 3.

$$\Delta G = RT \ln(p_{O_2}) \quad (10)$$

Where ΔG as the Gibbs free energy, R as the gas constant, p as the partial pressure, and T as the oxidation temperature in Kelvin.

The adhesion energy of the scale on a steel substrate can be calculated by equation (11) [44-46].

$$G = W \cdot \vartheta \quad (11)$$

Where G as the mechanical adhesion energy (J.m⁻²), W as the total stored energy in the oxide scale until the first spallation (J.m⁻³), and ϑ as the oxide scale thickness (m). The adhesion energy calculated in this work was predominantly depended on the scale thickness and strain initiating the first spallation to calculate stored energy. The scale thickness was measured directly from the cross-section SEM image. The result shows the mechanical adhesion energy of lower silicon steel was 281 J.m⁻² and 334 J.m⁻² for the higher silicon steel. This indicates that the scale adhesion on the 0.193 wt% Si steel was higher than that of scale on the 0.026 wt% Si steel, the higher silicon steel was shown to be strongly scale-adhered. The information about scale adhesion as reported in Table 4.

useful in the presence of silicon alloys in hot-rolled steel, which will affect the descaling process after the hot-rolling line. Therefore, the amount of elemental silicon should be added as low as possible.

Acknowledgements

This research was funded by National Science, Research, and Innovation Fund (NSRF), and King Mongkut's University of Technology North Bangkok with Contract no. KMUTNB-FF-65-09. Sahaviriya Steel Industries Public Company Limited for the provision of the hot-rolled steel strips for the study. The researcher would like to show my appreciation for being supported this research until it was accomplished very well.

References

- [1] L. Suarez, Y. Houbaert, X. V. Eynde, and R. Colás, "High temperature deformation of oxide scale," *Corrosion Science*, vol. 51, no. 2, pp. 309-315, 2009.
- [2] M. Krzyzanowski, J. H. Beynon, and D. C. Farrugia, *Oxide scale behavior in high temperature metal processing*. John Wiley & Sons, 2010.
- [3] S. Chandra-ambhorn, "Oxidation kinetics, mechanical adhesion and pickling behaviour of thermal oxide scales on hot-rolled conventional and recycled steels," *Steel Research Int.*, vol. 81, no. 9, pp. 130-133, 2010.
- [4] W. Noh, J. M. Lee, D. J. Kim, J. H. Song, and M. G. Lee, "Effects of the residual stress, interfacial roughness and scale thickness on the spallation of oxide scale grown on hot rolled steel sheet," *Materials Science and Engineering*, vol. A 739, pp. 301-316, 2019.
- [5] S. Liu, D. Tang, H. Wu, and L. Wang, "Oxide scales characterization of micro-alloyed steel at high temperature," *Journal of Materials Processing Technology*, vol. 213, no. 7, pp. 1068-1075, 2013.
- [6] Y. L. Yang, C. H. Yang, S. N. Lin, C. H. Chen, and W. T. Tsai, "Effects of Si and its content on the scale formation on hot-rolled steel strips," *Materials Chemistry and Physics*, vol. 112, no. 2, pp. 566-571, 2008.
- [7] D. Genève, D. Rouxel, P. Pigeat, and M. Confente, "Descaling ability of low-alloy steel wires depending on composition and rolling process," *Corrosion Science*, vol. 52, no. 4, pp. 1155-1166, 2010.
- [8] L. Suárez, P. Rodríguez-Calvillo, Y. Houbaert, and R. Colás, "Oxidation of ultra low carbon and silicon bearing steels," *Corrosion Science*, vol. 52, no. 6, pp. 2044-2049, 2010.
- [9] X. Yu, Z. Jiang, D. Wei, C. Zhou, Q. Huang, and D. Yang, "Tribological properties of magnetite precipitate from oxide scale in hot-rolled microalloyed steel," *Wear*, vol. 302, no. 1-2, pp. 1286-1294, 2013.
- [10] H. Utsunomiya, K. Hara, R. Matsumoto, and A. Azushima, "Formation mechanism of surface scale defects in hot rolling process," *CIRP Annals*, vol. 63, no. 1, pp. 261-264, 2014.
- [11] X. J. Liu, Y. Q. He, G. M. Cao, T. Jia, T. Z. Wu, and Z. Y. Liu, "Effect of Si content and temperature on oxidation resistance of Fe-Si alloys," *Journal of Iron and Steel Research International*, vol. 22, no. 3, pp. 238-244, 2015.
- [12] Q. Yuan, G. Xu, M. X. Zhou, and B. He, "New insights into the effects of silicon content on the oxidation process in silicon-containing steels," *International Journal of Minerals, Metallurgy, and Materials*, vol. 23, no. 9, pp. 1048-1055, 2016.
- [13] H. Utsunomiya, T. Nakagawa, and R. Matsumoto, "Mechanism of oxide scale to decrease friction in hot steel rolling," *Procedia Manufacturing*, vol. 15, pp. 46-51, 2018.
- [14] J. Eklund, B. Jönsson, A. Persdotter, J. Liske, J. E. Svensson, and T. Jonsson, "The influence of silicon on the corrosion properties of FeCrAl model alloys in oxidizing environments at 600°C," *Corrosion Science*, vol. 144, pp. 266-276, 2018.
- [15] T. Nishimoto, K. Honda, Y. Kondo, and K. Uemura, "Effects of Si Content on the Oxidation Behavior of Fe-Si Alloys in Air," *Materials Science Forum*, vol. 696, pp. 126-131, 2011.
- [16] X. J. Hu, B. M. Zhang, S. H. Chen, F. Fang, and J. Q. Jiang, "Oxide scale growth on high carbon steel at high temperatures," *Journal of Iron and Steel Research International*, vol. 20, no. 1, pp. 45-52, 2013.
- [17] C. Guan, J. Li, N. Tan, Y. Q. He, and S. G. Zhang, "Reduction of oxide scale on hot-rolled steel by hydrogen at low temperature," *International journal of hydrogen energy*, vol. 39, no. 27, pp. 15116-15124, 2014.
- [18] X. Yu, Z. Jiang, J. Zhao, D. Wei, C. Zhou, and Q. Huang, "Microstructure and microtexture evolutions of deformed oxide layers on a hot-rolled microalloyed steel," *Corrosion Science*, vol. 90, pp. 140-152, 2015.
- [19] Y. He, T. Jia, Z. Li, G. Cao, Z. Liu, and J. Li, "Isothermal reduction of oxide scale on hot-rolled, low-carbon steel in 10 pct H₂-Ar," *Metallurgical and Materials Transactions A*, vol. 47, no. 10, pp. 4845-4852, 2016.
- [20] R. Lu, G. Wu, and J. Zhang, "Effect of carbon on isothermal reduction of high-strength steel oxide scale in 30% H₂-N₂ atmosphere," *Journal of Cleaner Production*, vol. 279, p. 123681, 2021.
- [21] A. A. Mouayd, A. Koltsov, E. Sutter, and B. Tribollet, "Effect of silicon content in steel and oxidation temperature on scale growth and morphology," *Materials Chemistry and Physics*, vol. 143, no. 3, pp. 996-1004, 2014.
- [22] Q. Yuan, G. Xu, M. Zhou, and B. He, "The effect of the Si content on the morphology and amount of Fe₂SiO₄ in low carbon steels," *Metals*, vol. 6, no. 4, p. 94, 2016.
- [23] A. Chattopadhyay, and T. Chanda, "Role of silicon on oxide morphology and pickling behaviour of automotive steels," *Scripta Materialia*, vol. 58, no. 10, pp. 882-885, 2008.
- [24] M. Takeda, T. Onishi, S. Nakakubo, and S. Fujimoto, "Physical properties of iron-oxide scales on Si-containing steels at high temperature," *Materials transactions*, vol. 50, no. 9, pp. 2242-2246, 2009.
- [25] G. M. Martínez-Cázares, R. D. Mercado-Solís, R. Colás, and N. F. Garza-Montes-de-Oca, "High temperature oxidation of silicon and copper-silicon containing steels," *Ironmaking & Steelmaking*, vol. 40, no. 3, pp. 221-230, 2013.
- [26] Y. Yu, C. Wang, L. Wang, J. Chen, Y. J. Hui, and C. K. Sun, "Combination effect of Si and P on tertiary scale characteristic of hot rolled strip," *Journal of Iron and Steel Research International*, vol. 22, no. 3, pp. 232-237, 2015.
- [27] E. Ahtoy, M. Picard, G. Leprince, A. Galerie, Y. Wouters, X. Wang, and A. Atkinson, "Time and temperature dependence of the adhesion of oxide scales formed on phosphorus-containing steels during short term oxidation," *Materials Chemistry and Physics*, vol. 148, no. 3, pp. 1157-1162, 2014.
- [28] J. Liu and G. Jiang, "Use of laboratory indentation tests to study the surface crack propagation caused by various indenters," *Engineering Fracture Mechanics*, vol. 241, p. 107421, 2021.
- [29] M. M. Islam, S. I. Shakil, N. M. Shaheen, P. Bayati, and M. Haghshenas, "An overview of microscale indentation fatigue:

- Composites, thin films, coatings, and ceramics,” *Micron*, vol. 148, p. 103110, 2021.
- [30] Z. Cao, P. Wang, W. Gao, L. Tao, J. W. Suk, R. S. Ruoff, and K. M. Liechti, “A blister test for interfacial adhesion of large-scale transferred graphene,” *Carbon*, vol. 69, pp. 390-400, 2014.
- [31] H. Xin, R. Borduin, W. Jiang, K. M. Liechti, and W. Li, “Adhesion energy of as-grown graphene on copper foil with a blister test,” *Carbon*, vol. 123, pp. 243-249, 2017.
- [32] J. D. Hübsch, P. L. Rosendahl, C. Mittelstedt, “Blister tests on thin-walled composite structures at different temperatures,” *International Journal of Adhesion and Adhesives*, vol. 110, p. 102907, 2021.
- [33] M. Krzyzanowski and J. H. Beynon, “Modelling the behaviour of oxide scale in hot rolling,” *ISIJ international*, vol. 46, no. 11, pp. 1533-1547, 2006.
- [34] S. Chandra-Ambhorn, F. Roussel-Dherbey, F. Toscan, Y. Wouters, A. Galerie, and M. Dupeux, “Determination of mechanical adhesion energy of thermal oxide scales on AISI 430Ti alloy using tensile test,” *Materials science and technology*, vol. 23, no. 4, pp. 497-501, 2007.
- [35] Y. Kondo and H. Tanei, “Adhesive strength of oxide scale formed on low-carbon steel,” *Journal of the Japan Society for Technology of Plasticity*, vol. 54, no. 634, pp. 984-987, 2013.
- [36] C. Pascal, M. Braccini, V. Parry, E. Fedorova, M. Mantel, D. Oquab, and D. Monceau, “Relation between microstructure induced by oxidation and room-temperature mechanical properties of the thermally grown oxide scales on austenitic stainless steels,” *Materials Characterization*, vol. 127, pp. 161-170, 2017.
- [37] K. Ngamkham, S. Niltawach, and S. Chandra-Ambhorn, “Development of tensile test to investigate mechanical adhesion of thermal oxide scales on hot-rolled steel strips produced using different finishing temperatures,” *Key Engineering Materials*, vol. 462, pp. 407-412, 2011.
- [38] S. Chandra-ambhorn, K. Ngamkham, and N. Jiratthanakul, “Effects of process parameters on mechanical adhesion of thermal oxide scales on hot-rolled low carbon steels,” *Oxidation of metals*, vol. 80, no. 1, pp. 61-72, 2013.
- [39] G. Bamba, Y. Wouters, A. Galerie, F. Charlot, and A. Dellali, “Thermal oxidation kinetics and oxide scale adhesion of Fe-15Cr alloys as a function of their silicon content,” *Acta Materialia*, vol. 54, no. 15, pp. 3917-3922, 2006.
- [40] S. Vongsilathai, P. Thapanathitikul, K. Ngamkham, and T. Rojhirunsakool, “Effects of titanium and niobium on microstructure and mechanical adhesion of thermal oxide scales on hot-rolled low carbon steel,” *Suranaree Journal of Science & Technology*, vol. 26, no. 11, pp. 84-92, 2019.
- [41] D. J. Young, *High temperature oxidation and corrosion of metals*. Elsevier, 2008
- [42] Z. F. Li, Y. Gao, G. M. Cao, and Z. Y. Liu, “High-efficiency reduction behavior for the oxide scale formed on hot-rolled steel in a mixed atmosphere of hydrogen and argon,” *Journal of Materials Science*, vol. 55, no. 4, pp. 1826-1839, 2020.
- [43] P. Devkate, *High temperature oxidation of HSLA steel under vapor conditions*. 2019.
- [44] U. R. Evans, *An introduction to metallic corrosion*. Arnold, 1958.
- [45] H. E. Evans, “Stress effects in high temperature oxidation of metals,” *International materials reviews*, vol. 40, no. 1, pp. 1-40, 1995.
- [46] H. E. Evans, “Predicting oxide spallation from sulphur-contaminated oxide/metal interfaces,” *Oxidation of metals*, vol. 79, no. 1, pp. 3-14, 2013.